

Modified Risk Formulation for Improving the Prediction of Knee Osteoarthritis Progression

Haresh Rengaraj Rajamohan, MS¹, Richard Kijowski, MD², Kyunghyun Cho, PhD¹, Cem M.

Deniz, PhD^{2,3}

1. Center for Data Science, New York University, 60 5th Ave, New York, NY 10011
2. Department of Radiology, New York University Langone Health, 227 E 30th St, New York NY, 10016
3. Bernard and Irene Schwartz Center for Biomedical Imaging, New York University Langone Health, New York, NY, 10016, USA

Corresponding author:

Haresh Rengaraj Rajamohan,
New York University,
Center for Data Science,
60 Fifth Avenue, Room 227
New York, NY 10011, USA
Phone: (+1)-917-385-9479
Email: hrr288@nyu.edu

Summary Statement: A novel risk formulation improves the predictions of knee osteoarthritis progression to total knee replacement over multiple time horizons -12 months, 24 months and 48 months.

Key Results:

1. Our proposed constraint is effective at improving total knee replacement (TKR) prediction performance particularly within shorter time horizons.
- 2 The proposed modified risk formulation approaches demonstrate a significant improvement in predicting TKR over traditional methods across multiple time-horizons (12 months, 24 months and 48 months) on both MRIs and Radiograph datasets.
2. They further exhibit superior generalization capabilities on the external MOST dataset, with a consistently higher AUROC, AUPRC across all time horizons.
3. Application of the risk formulation through regularization methods appear to be inconsistent and ineffective at improving performance.

Abbreviations: OA: Osteoarthritis, MRI: Magnetic Resonance Imaging, TKR: Total Knee Replacement, DL: Deep Learning, CNN: Convolutional Neural Networks, OAI: Osteoarthritis Initiative, BMI: Body Mass Index, WOMAC: Western Ontario and McMaster Universities Osteoarthritis Index, KOOS QoL: Quality of Life from Knee Injury and Osteoarthritis Outcome, MOAKS: MRI Osteoarthritis Knee Score, 3D: Three-Dimensional, T1-TSE: T1-Weighted Turbo Spin-Echo, IW-TSE: Intermediate-Weighted Turbo Spin-Echo, DESS: Dual-Echo in Steady State, AUC: Area Under the Receiver Operating Characteristics Curve, AUPRC: Area Under the Precision-Recall Curve, OR: Odds Ratio

ABSTRACT

Background: Current methods for predicting osteoarthritis (OA) outcomes do not incorporate disease-specific prior knowledge to improve the outcome prediction models

Purpose: To effectively use consecutive imaging studies to improve OA outcome predictions by incorporating an OA severity constraint. The constraint enforces that the risk of OA for a knee should either increase or remain the same over time.

Materials and Methods: Participants of our retrospective study consisted of 364 case-control pairs of subjects from the Osteoarthritis Initiative (OAI) and Multicenter Osteoarthritis Study (MOST) with and without TKR over a 108-month follow-up period matched according to age, sex, ethnicity, and body mass index. DL models were trained to predict TKR within multiple time periods (1 year, 2 years, and 4-years) using knee radiographs and MRI scans. Models with and without risk constraint were evaluated using the area under the receiver operator curve (AUROC) and the area under the precision-recall curve (AUPRC) analysis.

Results: The novel RiskFORM2 method, leveraging a dual-model risk constraint architecture, demonstrated superior performance, yielding an Area Under the Receiver Operating Characteristic (AUROC) of 0.87 and Area Under the Precision-Recall Curve (AUPRC) of 0.47 for 1-year TKR prediction on the OAI radiograph test set—a marked improvement over the 0.79 AUROC and 0.34 AUPRC of the baseline non-risk-constraint approach. The performance advantage extended to longer follow-up periods, with RiskFORM2 maintaining a high AUROC of 0.86 and AUPRC of 0.75 at the 4-year mark. Additionally, when generalizing to the external MOST radiograph test set, RiskFORM2 achieved commendable robustness with an AUROC of 0.77 and AUPRC of 0.25 for 1-year predictions, which was higher than the 0.71 AUROC and 0.19 AUPRC of the baseline approach. In the MRI test sets, similar patterns emerged, with RiskFORM2 outperforming the baseline approach consistently. However,

RiskFORM1 exhibited the highest AUROC of 0.86 and AUPRC of 0.72 for 4-year predictions on the OAI set.

Conclusion: DL models trained with the proposed risk constraint had higher diagnostic performance for predicting TKR over shorter time periods than a DL model trained using conventional loss functions.

I. INTRODUCTION

Osteoarthritis (OA) is the most common form of arthritis and the major cause of physical disability in the elderly. OA causes a major socioeconomic burden with the overall costs associated with treatment of patients with the disease estimated to be 19,000 Euros per year¹. OA is generally diagnosed with the combination of clinical symptoms and radiographic findings of osteophyte formation and joint space loss. Predicting OA progression has previously been posed as a supervised learning problem with radiographs of the knee joints as inputs and various OA progression outcomes as labels to be predicted^{2,3,4}. Total knee joint replacement (TKR) to relieve pain and restore function in severely diseased knee joints is generally used at the endpoint of knee OA progression⁵. Prediction models for TKR outcome have been developed in the past to help determine which knees at baseline have high risk for undergoing future TKR.

In recent years, convolutional neural networks (CNNs) have been applied to predict the incidence and progression of knee OA, providing successful outcome prediction models. Tolpadi et al.² trained models with DenseNet⁶ architecture to predict the TKR outcome within 5 years using cross-entropy loss. Image-only models achieved an AUC of 0.85 for radiographs and 0.89 for magnetic resonance images. Tiulpin et al.⁷ trained a CNN model to predict OA based on Kellgren-Lawrence grade⁸ (KL-grade), which assesses the presence and severity of radiographic knee OA, and achieved a very high AUC of 0.93. Li et al used a Siamese architecture with a contrastive loss function to encode the severity of OA using the KL-grade. They found that the Siamese network outputs, which are the Euclidean distances between hidden representations of two knees, correlate well with both longitudinal change over time in disease severity and across patients with different KL-grades. Their approach, using the pairwise Euclidean distance achieves an AUC of 0.88 over time and 0.9 across patients. These results illustrate the effectiveness of CNN models in encoding OA severity for knee OA diagnosis.

Knee OA is a condition characterized by gradual progression of degeneration of cartilage and other joint structures. Given its progressive nature, the risk associated with OA typically escalates or remains constant over time; a decline in risk is highly unlikely as current treatments are not effective¹⁰. Our preliminary analysis using models employing plain cross-entropy loss for future TKR prediction failed to accurately adjust OA risk over time, underscoring the need for model training that align with the disease's progressive nature. For example, models predicting TKR within 9 years from Leung et al⁴ on average reduced their predicted risk over time in approximately 32% of the cases. To this end, we propose a risk constraint specific to knee OA that enforces the assumption that for a knee, the risk of TKR should either increase or remain the same over time. During training of the CNN model, this constraint was enforced between two scans of the same knee. Our hypothesis is that the use of the risk constraint would improve model performance for predicting TKR.

II. MATERIALS AND METHODS

A. Subject Cohort

Our retrospective study was performed using knees selected from subjects in the publicly available Osteoarthritis Initiative (OAI) and Multicenter Osteoarthritis Study (MOST) databases. The OAI database contains demographic and clinical information, radiographs, and MRI examinations from 4796 subjects between 45 and 79 years of age with or at risk for knee OA evaluated at baseline and 12, 24, 36, 48, 60, 72, 84, and 108-month follow-up. (14). The MOST database contains the same clinical information and imaging studies from 3026 subjects between 50 and 79 years of age with or at risk for knee OA evaluated at baseline and 15, 30, 60, 84-month follow-up. The OAI and MOST were approved by the Internal Review Boards at University of California at San Francisco, Boston University Medical Center, and each individual clinical recruitment site and were performed in compliance with the Health Insurance Portability and Accountability Act. All subjects signed written informed consent.

B. Training and Validation Group

Our analysis was conducted using two distinct datasets: one comprised of radiographs and the other comprised of MRI scans. To address the specific characteristics of each dataset, dedicated models were trained separately for the radiographs and MRI scans. These models were then evaluated on their corresponding test sets to compare model performance.

Training and validation groups from the OAI and MOST databases were selected to train the models to be invariant to clinical risk factors and use only features on radiographs or MRI to predict TKR. Balanced case-control cohorts were selected from both OAI and MOST sets by matching case subjects and control subjects with respect to baseline demographic variables associated with knee OA progression including age, sex, ethnicity, and body mass index (BMI). Case subjects were defined as individuals who underwent a TKR in either knee after the baseline enrollment date, while control subjects were defined as individuals who appeared at the 108-month follow-up, or 84-month follow-up visit and had not undergone a TKR in either knee. If a patient underwent TKR in both knees during OAI data collection, the knee that first underwent TKR was included. Each case patient with TKR was matched to a control subject without TKR who had the same age, sex, and ethnicity, with an additional constraint on the baseline BMI within a 10% tolerance. The data set from case-control pairs contained either the left or right knee from each case and control subject.

Two datasets from the OAI were created: one comprised of radiographs and the other comprised of MRI scans. A total of 364 case-control pairs with a baseline radiograph were identified from the 4796 subjects in the OAI database. Only 353 of these 364 case-control pairs had baseline MRI scans. Subjects were excluded if they had TKR at baseline, received partial TKR over the course of follow-up, had inflammatory arthritis, were missing baseline or 108-month follow-up information, or did not match with

a case or control subject. For the MRI models, the coronal intermediate-weighted turbo spin-echo (COR IW-TSE) sequence in the MRI scans were used for training and validating the models.

The data from Multicenter Osteoarthritis Study (MOST) was used to test the generalization capabilities of the trained models. Similar to the OAI, two datasets were created: one comprised of radiographs and the other comprised of MRI scans. A total of 574 case-control pairs with baseline radiographs were identified from the 3026 subjects in the MOST database. Only 378 of these case-control pairs had baseline MRI. The same exclusion criteria as OAI were used here except the last follow-up information was at 84 months instead of 108 months from the baseline. For the MRI models, the short-tau inversion recovery (COR STIR) sequence in the MRI scans were used for training and validating the models.

In both the OAI and MOST datasets, for each subject's knee, 2 images were used during training: the first radiograph or MRI was performed at baseline and the second radiograph or MRI scan was performed at the last available follow-up period before TKR, which occurred between 1 year and 4 years before the procedure. The use of two images was required in order to apply the risk constraint, which was based on the assumption that TKR risk on the second image was greater than or equal to the TKR risk on the first image. In order to increase the training and validation dataset size, knees with only one available radiograph or MRI scan (only the baseline) were also included. When training models on these single-image instances, the methodology was limited to applying the standard cross-entropy loss function, as the risk constraint, which requires a future scan, could not be applied.

A summary of the selection of case-control pairs for MRI and radiographs on the OAI and MOST set is illustrated in Figures 1 and 2. Study cohort characteristics are summarized in Table 1.

B.1 Prediction Tasks

The models were trained to predict the following Total Knee Replacement (TKR) outcomes.

- **1-year TKR prediction** – For a knee radiograph or MRI model, the model predicted if the subject underwent TKR within 1 year after both the baseline and the second knee radiograph or MRI scan.
- **2-years TKR prediction** – For a knee radiograph or MRI model, the model predicted if the subject underwent TKR within 2-year after both the baseline and the second knee radiograph or MRI scan.
- **4-years TKR prediction** – For a knee radiograph or MRI model, the model predicted if the subject underwent TKR within 4-years after both the baseline and the second knee radiograph or MRI scan.

C. Total Knee Replacement Risk Constraints

C.1. Modified Risk Formulation

If the constraint is enforced via regularization, there is still a possibility that it can be violated for a subset of knees. In order to strictly enforce the condition that TKR risk increases or remains the same over time, the TKR risk formulation was modified in the following way which is referred to as **RiskFORM1**.

$$p(x_1) = \hat{y}_t^1 = \sigma(f(x_1))$$

$$p(x_2, x_1) = \hat{y}_t^2 = 1 - p(x_1) * (1 - \sigma(f(x_2))) = 1 - (1 - \sigma(f(x_1))) * (1 - \sigma(f(x_2)))$$

Note that with this formulation, for any $f(x_1), f(x_2) \in R$, provides the desired property that $\hat{y}_t^1 \leq \hat{y}_t^2$.

The proof is simply as follows: since $(1 - \sigma(f(x_1))) \in (0,1)$

$$p(x_1) * (1 - \sigma(f(x_1))) \leq p(x_1)$$

which means,

$$\begin{aligned} 1 - p(x_1) * (1 - \sigma(f(x_1))) &\geq 1 - p(x_1) \\ \Rightarrow p(x_2, x_1) &\geq p(x_1) \end{aligned}$$

Here, the predicted risk on the first radiograph or MRI scan is explicitly utilized to compute the risk on the second radiograph or MRI scan, which can be interpreted as conditioning the probability of the second image on the first image.

Additionally, instead of using a single model f , formulation was used, referred to as **RiskFORM2**, which trains two models f, g and the TKR risks are given by,

$$p(x_1) = \hat{y}_t^1 = \sigma(f(x_1))$$

$$p(x_2, x_1) = \hat{y}_t^2 = 1 - p(x_1) * (\sigma(g(x_2))) = 1 - (1 - \sigma(f(x_1))) * (\sigma(g(x_2)))$$

The final loss function used here is simply,

$$L_{total} = BCE(y_t^1, \hat{y}_t^1) + BCE(y_t^2, \hat{y}_t^2)$$

In the case of a knee having a single radiograph or MRI scan, the TKR risk is \hat{y}_t^1 and the loss $L_{total} = BCE(y_t^1, \hat{y}_t^1)$ is applied during training. The TKR risk for the radiographs or MRI scan is computed in the aforementioned way during both training and evaluation as shown in Figure 3.

C.2 Risk Constraint Via Regularization

To compare our model to the pre-existing approaches, the risk constraint was applied via regularization loss function. Li et al applied contrastive loss with Siamese architecture for the prediction of KL-grades for knee radiographs and showed that the contrastive loss can successfully encode OA severity over time. So, an additional loss (**ConReg**) with Siamese architecture was used to enforce our constraint as shown in Figure 3. Another regularization approach called **RiskReg** was applied, where the risk constraint was directly applied on the models' outputs with a margin loss as shown in Figure 4. More detailed explanation of these regularization approaches is provided in the Appendix.

C.2 Baseline Approach

Furthermore, baseline radiograph and MRI models were trained to predict TKR risk using the cross-entropy loss without any constraints for comparison with the risk constraint approaches.

D. Model Training and Validation

The radiograph and MRI models were trained to predict TKR within 1-year, 2-years, and 4-years using 2 radiographs or MRI scans of each subject's knee recorded over a time period of at least 12 months. The OAI set was split in a stratified manner into 7 folds and nested cross-validation (CV) was used in training all the approaches. For the radiograph models, resnet34 architecture was used with ImageNet pre-trained initialization. For the MRI models, 3D resnet18 with He initialization¹¹ was used along with Adam optimizer¹². In 7-fold nested CV, 6 models were trained per fold with each fold used as a test set, and all the models were saved based on the best overall AUC on their respective validation sets. So, a total of 42 models were trained for each approach. For training the RiskReg models, a margin of 2 and gamma 1 were chosen based on preliminary hyperparameter tuning experiments.

During evaluation of the radiograph and MRI models for the OAI cohort, each fold was evaluated by an ensemble of its corresponding 6 trained models, and the metrics were computed over the entire cohort.

During evaluation of the radiograph and MRI models for the MOST cohort, all the 42 trained models were ensembled, and the metrics were computed over the entire cohort. For model evaluation, the Area Under the receiver operator Curve (AUROC) and the Area Under the Precision-Recall Curve (AUPRC) metrics were computed.

III. RESULTS

For both radiographs and MRI scans, the modified risk formulation approach outperformed the baseline and RiskReg approaches (Table 2). On the OAI radiograph test set, RiskFORM2, which used two models, achieved the best performance with AUROC 0.87 and AUPRC 0.47 on 1-year TKR prediction, AUROC 0.85 and AUPRC 0.63 on 2-years TKR prediction, and AUROC 0.86 and AUPRC 0.75 on 4-years TKR prediction compared to the baseline approach with AUROC 0.79 and AUPRC 0.34 on 1-year TKR prediction, AUROC 0.82 and AUPRC 0.52 on 2-years TKR prediction, and AUROC 0.85 and AUPRC 0.7 on 4-years TKR prediction. RiskFORM1 which uses a single model, also outperformed the baseline approach achieving AUROC 0.8 and AUPRC 0.39 on 1-year TKR prediction, AUROC 0.83 and AUPRC 0.58 on 2-years TKR prediction, and AUROC 0.85 and AUPRC 0.72 on 4-years TKR prediction.

RiskFORM2 also had better generalization than the baseline and RiskReg approaches to the external MOST radiograph test set, with slight degradation in performance across the board compared to the OAI test set. RiskFORM2 again achieved the best results with AUROC 0.77 and AUPRC 0.25 on 1-year TKR prediction, AUROC 0.79 and AUPRC 0.43 on 2-years TKR prediction, and AUROC 0.81 and AUPRC 0.63 on 4-years TKR prediction. In comparison, the baseline approach achieved AUROC 0.71 and AUPRC 0.19 on 1-year TKR prediction, AUROC 0.75 and AUPRC 0.39 on 2-years TKR prediction, and AUROC 0.79 and AUPRC 0.59 on 4-years TKR prediction. RiskFORM1 also generalized better than the baseline approach achieving AUROC 0.78 and AUPRC 0.23 on 1-year TKR prediction, AUROC 0.78 and AUPRC 0.41 on 2-years TKR prediction, and AUROC 0.81 and AUPRC 0.63 on 4-years TKR prediction. The improvement of RiskFORM2 compared to the baseline approach for the OAI test set decreased as the time period between the last radiograph and TKR increased, but RiskFORM2 showed considerable improvement over all time periods on the MOST test set.

On the MRI test sets, similar trends were observed for both the COR IW TSE sequence in the OAI and the coronal COR STIR sequence in MOST, with RiskFORM2 achieving the best performance in general. RiskFORM2 achieved an AUROC 0.80 and AUPRC 0.39 on 1-year TKR prediction, AUROC 0.83 and AUPRC 0.58 on 2-years TKR prediction, and AUROC 0.85 and AUPRC 0.72 on 4-years TKR prediction in the OAI test set and AUROC 0.78 and AUPRC 0.23 on 1-year TKR prediction, AUROC 0.78 and AUPRC 0.41 on 2-years TKR prediction, and AUROC 0.81 and AUPRC 0.63 on 4-years TKR prediction in the MOST test set. However, for the 4-year TKR prediction in the OAI test set, RiskFORM1 achieved the best performance with AUROC 0.86 and AUPRC 0.72. Once again, improvement of RiskFORM2 compared to the baseline approach for the OAI test set decreased as the time period between the last radiograph and TKR increased, but RiskFORM2 showed considerable improvement over all time periods on the MOST test set.

Enforcing the constraint via regularization in the RiskReg, and ConReg approaches resulted in worse AUCs and AUPRCs in comparison to the baseline approach. On the radiograph test set, ConReg appeared to be slightly effective, achieving good generalization to the MOST test set with AUROC 0.76 and AUPRC 0.2 on 1-year TKR prediction, AUROC 0.77 and AUPRC 0.39 on 2-years TKR prediction, and AUROC 0.8 and AUPRC 0.6 on 4-years TKR prediction compared to baseline approach. However, in the MRI test set for both OAI and MOST, ConReg appeared to be ineffective and consistently underperformed the baseline approach. RiskReg the combination of RiskReg and ConReg both underperformed the baseline approach across the board.

IV. DISCUSSION

This study showed that the modified risk formulation approaches, specifically and RiskFORM1 and RiskFORM2, significantly outperformed the baseline approach and RiskReg approaches for predicting

TKR across various time periods. On the radiograph OAI test set, RiskFORM2 demonstrated superior performance, particularly for 1-year TKR prediction, with an AUROC of 0.87 and AUPRC of 0.47, and showed consistent improvement across 2-year and 4-year TKR predictions. RiskFORM1 also surpassed the baseline approach but with marginally lower performance than RiskFORM2. These trends held when models were tested on an external MOST testing set, although with a slight performance decrease.

The Modified risk formulation enhances the performance of TKR prediction models by essentially integrating longitudinal data. Unlike the baseline approach, which treat imaging studies independently, this approach conditions the risk prediction on a previous scan, thereby utilizing a broader spectrum of subject data to better inform the risk prediction. This additional temporal context provides a more nuanced understanding of disease progression, crucial for accurate risk assessment in a progressive disease such as OA. RiskFORM 2 utilizes two separate models to independently process image 1 and image 2, while RiskFORM 1 employs a single shared model for both images. The dual-model approach of RiskFORM 2 allows for greater flexibility in risk adjustment between the two images, leading to improved performance compared to RiskFORM 1. Furthermore, the superior performance of the modified risk formulation models on the MOST test set suggests that incorporating the risk constraint improves model generalization and robust to changes in data distribution. Our study opens an interesting line of research into coming up with new risk formulations that can condition on more than one past scan in a scalable and efficient manner.

Interestingly, the relative improvement of RiskFORM1 and RiskFORM2 over the baseline approach decreased as the time period between TKR and the last radiograph or MRI scan was performed increased for both the OAI and MOST test sets. However, the modified risk formulation approaches still provided some performance improvements for the 4-year TKR prediction, especially for the MOST test set. This decrease in model performance may be attributed to a reduction in number of knees available for model training as the number of subjects transitioning from TKR-negative in the first image (i.e. baseline image)

to TKR-positive in the second image (i.e. last available follow-up image) decreased as the TKR time horizon increased. However, still RiskFORM demonstrated its utility at the 4-year TKR prediction, showing persistent improvements compared to the baseline model which did not adjust its predictions between two subtly different images, typically. Conversely, the RiskFORM approaches are specifically designed to account for these nuanced differences between the baseline and follow-up images, thereby improving model performance.

In the MRI dataset, similar patterns emerged, with RiskFORM2 generally achieving the highest performance metrics. However, for the 4-year TKR predictions, RiskFORM1 unexpectedly outperformed both the baseline approach and RiskFORM2 on the OAI test set. Given that MRI data is three-dimensional and inherently more complex than radiographs, coupled with a smaller training set, there is an increased risk of overfitting with RiskFORM2, which trains two models, compared to the single model used in RiskFORM1. Another reason could be due to artifacts present in our MRI exams. In contrast, regularization strategies such as RiskReg and ConReg did not improve upon the baseline approach and in some instances led to lower performance, particularly when evaluating the MRI scans. This suggests that the added complexity introduced by these approaches may not align well with the underlying data characteristics or model structures.

Previously, Kim et al.¹⁵ introduced PairNet, a pairwise image ranking network designed to order two medical images from the same patient by identifying which image was captured later. The prediction is made based on the difference between the predicted representations from the network's final layer on two image inputs. This serves as a regularization, forcing the model to accurately predict the rank using cross entropy loss function, like RiskReg and ConReg. However, this framework was used exclusively in self-supervised learning and not directly in supervised learning applications. In the realm of supervised learning, the investigators used a similar strategy but only for regression tasks that involve continuous labels such as tumor size, which continuously vary over time - unlike the binary classification in our

work. This method was demonstrated to be effective for predicting brain age, a task where changes over time are incorporated into the label unlike in binary classification. To the best of our knowledge, our work is the first to introduce a risk formulation modification to incorporate severity constraints, making it applicable to a wide variety of longitudinal progressive disease datasets, not limited to scenarios with continuously changing labels.

In a previous study, Leung et al.⁴ utilized ResNet34-based CNN models for predicting knee OA outcomes, including Kellgren-Lawrence (KL) grades and 9-year TKR, achieving AUCs of 0.87 for predicting TKR and over 0.80 for predicting KL grades. Our current analysis showed a decline in TKR prediction performance when the follow-up time period shortened from 9 years to 4 years or less. The lower model performance may stem from two factors: First, the datasets were not identical. While Leung et al.⁴ used only baseline radiographs from the OAI dataset, our study incorporated additional image data including sequentially performed radiographs and MRI scans. Secondly, as illustrated by COVID-19 progression prediction models from Shamout et al.¹³ that performed optimally over a 96-hour horizon compared to shorter 24h, 48h and 72h time period, shortening the labeling time period could blur the distinction between positive and negative cases. As a result, the model would need to discriminate more acutely between moderate and relatively severe OA on radiographs and MRI.

There are several limitations to our study. In both the OAI and MOST datasets, the knee radiographs were acquired in a systematic way, which might not be reflective of real-world imaging data. Further studies are needed for the successful translation of the developed models into the real-world clinical setting where radiographs and MRI are acquired using different imaging systems and protocols. Another limitation was that the datasets contained class imbalance due to the slow-progressing nature of OA. The much larger number of knees without TKR than knees with TKR could limit model training and potentially affect model performances toward specific types of TKR case knees.

In conclusion, our study showed that DL models trained with the proposed risk constraint had higher performance for predicting TKR over shorter time periods than a baseline DL model trained using conventional loss functions. The proposed model training method could benefit the research community and be applied to risk assessment models for other progressive diseases. Models trained for the prediction of progression-based outcomes both in and outside the domain of OA could incorporate this formulation to improve their performance and generalizability.

Tables

Modality	Cohort	# of Patient Knees	# of Images	# of males	# of females	Age (mean \pm std)	BMI (mean \pm std)
Radiograph	OAI	728	1428	284	444	63.6 \pm 8.2	29.8 \pm 4.6
	MOST	1148	2061	352	796	64.3 \pm 7.4	31.8 \pm 5.5
MRI	OAI	708	1372	276	432	63.7 \pm 8.2	29.7 \pm 4.5
	MOST	756	1328	180	576	64.9 \pm 7.3	31.8 \pm 5.5

Table 1: Distribution of patients on the OAI and MOST sets.

	TE (ms)	TR (ms)	TI (ms)	FOV (mm)	ST (mm)	ISR (mm²)	Matrix Size	Bandwidth (Hz/pixel)
COR IW-TSE	20	3700	NA	140	3.0	0.36x0.36	384x384	352
COR STIR	35	4800	100	140	3.0	0.55x0.72	256x192	NS

Table 2: Imaging parameters of the coronal T1-weighted turbo spin-echo (COR IW-TSE) sequences performed in the MRI examination of subjects in the OAI database, and the coronal short-tau inversion recovery (COR STIR) sequences performed in the MRI examination of subjects in the MOST database.

	1 year TKR				2 years TKR				4 years TKR			
	OAI		MOST		OAI		MOST		OAI		MOST	
	AUC (95% CI)	AUPRC (95% CI)										
Base	0.79 (0.76, 0.83)	0.34 (0.29, 0.41)	0.71 (0.68, 0.75)	0.19 (0.16, 0.24)	0.83 (0.81, 0.86)	0.54 (0.49, 0.61)	0.75 (0.73, 0.78)	0.39 (0.35, 0.44)	0.85 (0.82, 0.87)	0.70 (0.65, 0.75)	0.79 (0.77, 0.81)	0.59 (0.55, 0.63)
RiskReg	0.79 (0.76, 0.83)	0.34 (0.29, 0.40)	0.72 (0.69, 0.76)	0.18 (0.15, 0.21)	0.81 (0.79, 0.84)	0.52 (0.46, 0.58)	0.76 (0.73, 0.78)	0.38 (0.34, 0.43)	0.84 (0.81, 0.86)	0.68 (0.63, 0.73)	0.80 (0.78, 0.82)	0.60 (0.56, 0.64)
ConReg	0.83 (0.80, 0.86)	0.38 (0.33, 0.45)	0.76 (0.73, 0.79)	0.20 (0.17, 0.25)	0.83 (0.81, 0.86)	0.55 (0.49, 0.61)	0.77 (0.75, 0.79)	0.39 (0.35, 0.44)	0.85 (0.83, 0.87)	0.70 (0.65, 0.74)	0.80 (0.78, 0.82)	0.60 (0.56, 0.64)
ConReg + RiskReg	0.81 (0.78, 0.84)	0.35 (0.30, 0.42)	0.73 (0.70, 0.76)	0.19 (0.16, 0.24)	0.83 (0.80, 0.85)	0.52 (0.46, 0.58)	0.76 (0.74, 0.78)	0.39 (0.34, 0.44)	0.84 (0.82, 0.86)	0.70 (0.65, 0.74)	0.81 (0.79, 0.83)	0.62 (0.58, 0.66)
RiskFORM2	0.87 (0.84, 0.89)	0.47 (0.40, 0.55)	0.77 (0.74, 0.81)	0.25 (0.20, 0.30)	0.85 (0.83, 0.88)	0.63 (0.57, 0.70)	0.79 (0.77, 0.82)	0.43 (0.38, 0.48)	0.86 (0.84, 0.88)	0.75 (0.71, 0.80)	0.81 (0.79, 0.83)	0.63 (0.59, 0.67)
RiskFORM1	0.80 (0.77, 0.83)	0.39 (0.33, 0.47)	0.78 (0.75, 0.81)	0.23 (0.19, 0.28)	0.83 (0.80, 0.85)	0.58 (0.52, 0.64)	0.78 (0.75, 0.80)	0.41 (0.36, 0.46)	0.85 (0.82, 0.87)	0.72 (0.68, 0.77)	0.81 (0.79, 0.83)	0.63 (0.59, 0.67)

Table 3: Results comparing the various risk constraint methods with the baseline model on the OAI and MOST radiograph test sets.

	1 year TKR				2 years TKR				4 years TKR			
	OAI		MOST		OAI		MOST		OAI		MOST	
	AUC (95% CI)	AUPRC (95% CI)	AUC (95% CI)	AUPRC (95% CI)	AUC (95% CI)	AUPRC (95% CI)	AUC (95% CI)	AUPRC (95% CI)	AUC (95% CI)	AUPRC (95% CI)	AUC (95% CI)	AUPRC (95% CI)
Baseline	0.79 (0.76 , 0.83)	0.34 (0.28 , 0.42)	0.70 (0.65 , 0.75)	0.17 (0.12 , 0.23)	0.82 (0.79 , 0.85)	0.52 (0.46, 0.60)	0.66 (0.62 , 0.69)	0.24 (0.21, 0.29)	0.84 (0.82 , 0.86)	0.71 (0.66 , 0.75)	0.58 (0.55 , 0.61)	0.35 (0.32 , 0.39)
RiskReg	0.80 (0.76 , 0.83)	0.34 (0.28 , 0.42)	0.68 (0.63 , 0.72)	0.14 (0.11 , 0.20)	0.83 (0.80 , 0.86)	0.54 (0.48, 0.61)	0.62 (0.58 , 0.66)	0.21 (0.18, 0.25)	0.84 (0.82 , 0.86)	0.71 (0.66 , 0.75)	0.59 (0.56 , 0.62)	0.35 (0.32 , 0.39)
ConReg	0.78 (0.74 , 0.81)	0.34 (0.28 , 0.42)	0.70 (0.65 , 0.74)	0.17 (0.12 , 0.24)	0.83 (0.80 , 0.86)	0.54 (0.47, 0.61)	0.60 (0.56 , 0.64)	0.21 (0.18, 0.24)	0.85 (0.83 , 0.87)	0.71 (0.66 , 0.75)	0.58 (0.55 , 0.62)	0.36 (0.33 , 0.40)
ConReg + RiskReg	0.81 (0.78 , 0.84)	0.38 (0.32 , 0.46)	0.70 (0.65 , 0.75)	0.16 (0.12 , 0.22)	0.84 (0.81 , 0.86)	0.55 (0.48, 0.62)	0.62 (0.59 , 0.66)	0.22 (0.19, 0.26)	0.84 (0.81 , 0.86)	0.70 (0.65 , 0.74)	0.56 (0.53 , 0.59)	0.34 (0.31 , 0.38)
RiskFORM2	0.84 (0.80 , 0.87)	0.43 (0.35 , 0.51)	0.72 (0.67 , 0.77)	0.19 (0.14 , 0.27)	0.84 (0.81 , 0.87)	0.59 (0.53, 0.66)	0.66 (0.62 , 0.69)	0.27 (0.23, 0.32)	0.84 (0.82 , 0.86)	0.72 (0.68 , 0.77)	0.59 (0.56 , 0.62)	0.38 (0.34 , 0.42)
RiskFORM1	0.80 (0.77 , 0.83)	0.35 (0.29 , 0.43)	0.69 (0.64 , 0.74)	0.14 (0.11 , 0.19)	0.84 (0.82 , 0.87)	0.57 (0.51, 0.64)	0.66 (0.63 , 0.70)	0.24 (0.21, 0.29)	0.86 (0.83 , 0.88)	0.72 (0.68 , 0.77)	0.58 (0.55 , 0.62)	0.36 (0.32 , 0.40)

Table 4: Results comparing the various risk constraint methods with the baseline model on the OAI (COR IW-TSE) and MOST MRI (COR STIR) test sets.

Figures

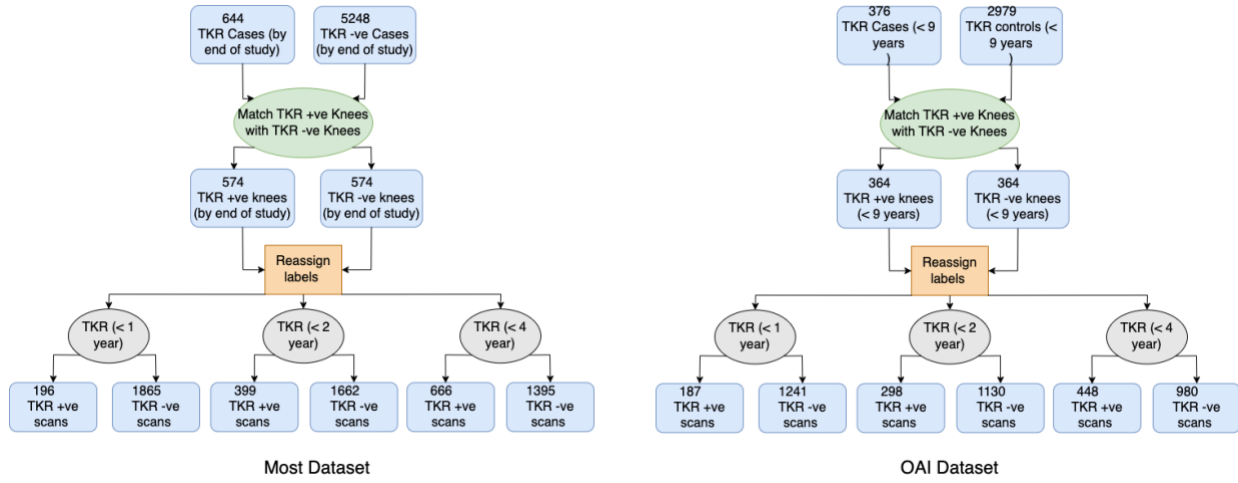


Figure 1: Radiograph Cohort selection pipeline for the MOST and OAI datasets

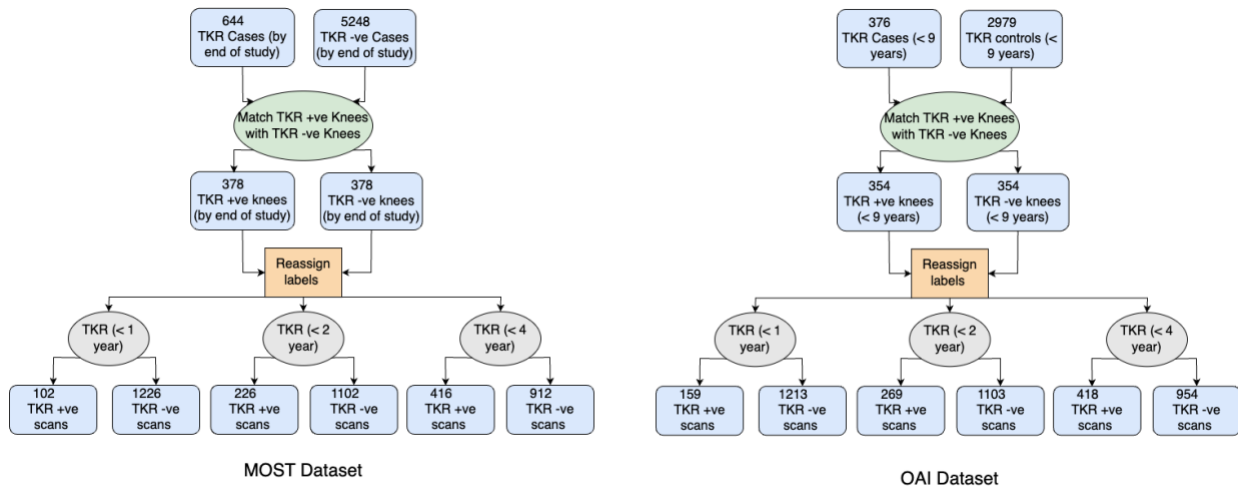
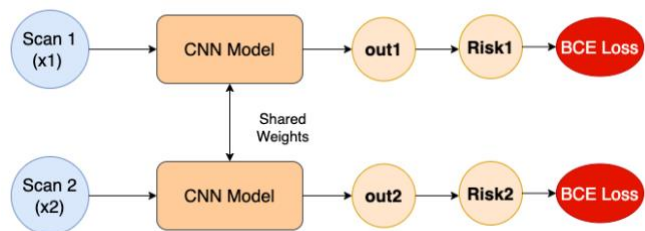
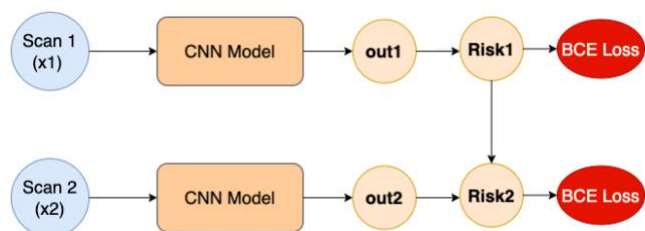


Figure 2: MRI Cohort selection pipeline for the MOST and OAI datasets

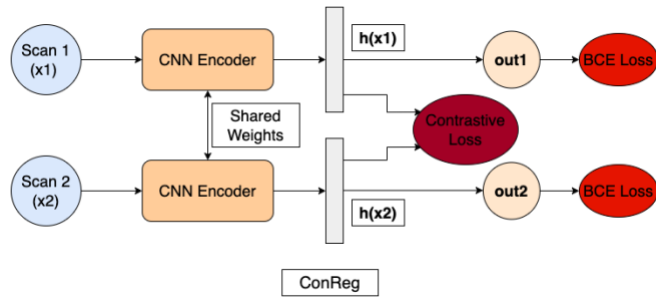


(a)

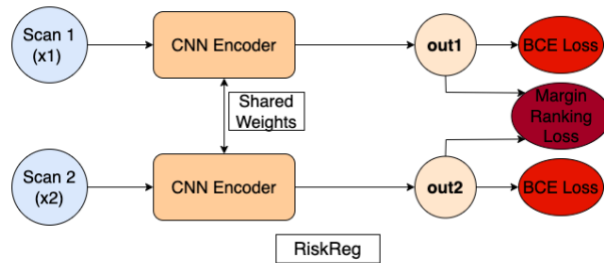


(b)

Figure 3: (a) The Baseline training approach without any risk constraint. (b) The proposed modified risk formulation scheme that effectively conditions on past scan.



(a)



(b)

Figure 4: Regularization methods for enforcing the risk constraint (a) ConReg via Siamese loss and (b) RiskReg via margin loss.

References

1. Cross, Marita, et al. "The global burden of hip and knee osteoarthritis: estimates from the global burden of disease 2010 study." *Annals of the rheumatic diseases* 73.7 (2014): 1323-1330.
2. Tolpadi, Aniket A., et al. "Deep learning predicts total knee replacement from magnetic resonance images." *Scientific reports* 10.1 (2020): 6371.
3. Zhang, Bofei, et al. "Attention-based cnn for kl grade classification: Data from the osteoarthritis initiative." *2020 IEEE 17th international symposium on biomedical imaging (ISBI)*. IEEE, 2020.

4. Leung, Kevin, et al. "Prediction of total knee replacement and diagnosis of osteoarthritis by using deep learning on knee radiographs: data from the osteoarthritis initiative." *Radiology* 296.3 (2020): 584-593.
5. Dougados, Maxime, et al. "OARSI/OMERACT criteria of being considered a candidate for total joint replacement in knee/hip osteoarthritis as an endpoint in clinical trials evaluating potential disease modifying osteoarthritic drugs." *The Journal of Rheumatology* 36.9 (2009): 2097-2099.
6. Huang, Gao, et al. "Densely connected convolutional networks." *Proceedings of the IEEE conference on computer vision and pattern recognition*. 2017.
7. Tiulpin, Aleksei, et al. "Automatic knee osteoarthritis diagnosis from plain radiographs: a deep learning-based approach." *Scientific reports* 8.1 (2018): 1727.
8. Kellgren, Jonas H., and JS1006995 Lawrence. "Radiological assessment of osteoarthritis." *Annals of the rheumatic diseases* 16.4 (1957): 494.
9. He, Kaiming, et al. "Deep residual learning for image recognition." *Proceedings of the IEEE conference on computer vision and pattern recognition*. 2016
10. Karsdal, M. A., et al. "Disease-modifying treatments for osteoarthritis (DMOADs) of the knee and hip: lessons learned from failures and opportunities for the future." *Osteoarthritis and cartilage* 24.12 (2016): 2013-2021.
11. He, Kaiming, et al. "Delving deep into rectifiers: Surpassing human-level performance on imagenet classification." *Proceedings of the IEEE international conference on computer vision*. 2015.
12. Kingma, Diederik P., and Jimmy Ba. "Adam: A method for stochastic optimization." *arXiv preprint arXiv:1412.6980* (2014).
13. Shamout, Farah E., et al. "An artificial intelligence system for predicting the deterioration of COVID-19 patients in the emergency department." *NPJ digital medicine* 4.1 (2021): 80.
14. Weston, Jason, and Chris Watkins. "Support vector machines for multi-class pattern recognition." *Esann*. Vol. 99. 1999.
15. Kim, Heejong, and Mert R. Sabuncu. "Learning to compare longitudinal images." *arXiv preprint arXiv:2304.02531* (2023).

Appendix

ConReg

In this setting for two scans x_1, x_2 and model f , the predicted representations at the penultimate layer (h_1, h_2) are obtained and used to compute the contrastive loss.

$$L_{cont} = y_{siam} * \|h_2 - h_1\|^2 + (1 - y_{siam}) * ((0, m - \|h_2 - h_1\|)^2)$$

Where y_{siam} is the Siamese label with $y_{siam} = 1$ if $y_t^1 = y_t^2$ and $y_{siam} = 0$ if $y_t^1 \neq y_t^2$. So effectively the representations of the two scans are pushed together if their TKR labels are the same and they are pushed apart if their TKR labels are different. The total loss applied here is,

$$L_{total} = BCE(y_t^1, \hat{y}_t^1) + BCE(y_t^2, \hat{y}_t^2) + \gamma * L_{cont}$$

RiskReg

The loss regularization approach (**RiskReg**) to the application of risk constraint is formalized below. For a knee, we have a scan from time step 1 (x_1), a scan from time step 2 (x_2) and a CNN model (f). The risk of TKR within t years for these two scans is given by,

$$p(x_1) = \hat{y}_t^1 = \sigma(f(x_1))$$

$$p(x_2) = \hat{y}_t^2 = \sigma(f(x_2))$$

where σ is the logistic sigmoid function, $y_t^1, y_t^2 \in \{0,1\}$ indicating the true TKR status in t years for scans at time-step 1 and time-step 2 respectively, $t \in \{1,2,4\}$ in this study, $f(x_1), f(x_2) \in R$, $\sigma(f(x_1)), \sigma(f(x_2)) \in (0,1)$, and \hat{y}_t^1, \hat{y}_t^2 are the predicted TKR risks.

As stated earlier, our assumption is $p(x_1) \leq p(x_2)$, which translates to

$$\sigma(f(x_1)) \leq \sigma(f(x_2))$$

This constraint is enforced by adding a margin ranking loss term¹⁴.

$$L_{reg} = \max(0, \log \log(\sigma(f(x_1))) - \log \log(\sigma(f(x_2)))) + m).$$

enforces the constraint $\log \log (\sigma(f(x_1))) - \log \log (\sigma(f(x_2))) \geq m$, where m is the margin hyperparameter that controls how far apart the log sigmoid outputs should be (as m is increased $\sigma(f(x_2))$ would be pushed farther away from $\sigma(f(x_1))$). The natural log (a strictly increasing function) is applied to the sigmoid output to achieve better numerical performance and avoid diminishing gradient problems associated with the sigmoid function during training. So, the total loss applied for a knee with two scans is,

$$L_{total} = BCE(y_t^1, \hat{y}_t^1) + BCE(y_t^2, \hat{y}_t^2) + \gamma * L_{reg}$$

Where BCE is the binary cross entropy loss. For a knee with only one scan, the $L_{total} = BCE(y_t^1, \hat{y}_t^1)$ is applied during training.